Available online at www.sciencedirect.com
ScienceDirect
Journal of Power Sources 168 (2007) 426–433
JOURNAL OF POWER SOURCES
www.elsevier.com/locate/jpowsour

Novel alkaline earth silicate sealing glass for SOFC Part I. The effect of nickel oxide on the thermal and mechanical properties

Yeong-Shyung Chou [a,*], Jeffry W. Stevenson [a], Robert N. Gow [b]

[a] *Pacific Northwest National Laboratory, Richland, WA 99354, United States*
[b] *Office of Science, Community College Institute, Montana Tech, MT 59701, United States*

Received 12 February 2007; received in revised form 14 March 2007; accepted 14 March 2007
Available online 23 March 2007

Abstract

This is a two-part study of a novel Sr–Ca–Ni–Y–B silicate sealing glass for solid oxide fuel cells (SOFC). In this paper (Part I), the effect of NiO on glass forming, thermal, and mechanical properties was studied with two different approaches: glass making and composite glass. In the following paper (Part II), sealing and interfacial microstructure of candidate composite glass with 10 vol.% NiO will be addressed. In Part I, higher NiO content in the glass resulted in precipitation during the glass making process, and the sintered powder compacts of these glasses showed extensive macro- and micro-cracks. Coefficient of thermal expansion (CTE) showed large decrease for glass with higher NiO contents. On the other hand, glass-based composites showed no fracture even with NiO content as high as 15 vol.%. The CTE of the composite glass, which increased with increasing NiO content (consistent with the rule of mixtures prediction), could be adjusted to match the CTE of SOFC components. Phase characterization by XRD identified phases of YBO_3 and NiO in the glass, which were likely responsible for the poor mechanical and thermal properties for the glass making approach.

Keywords: Glass seal; SOFC; Leak rate; NiO; CTE

1. Introduction

Solid oxide fuel cells (SOFCs) have been extensively studied in the last decade due to their high energy efficiency, high power density per unit volume, low noise, capability for internal fuel reforming, and near zero emissions [1]. In SOFCs, electrical energy is extracted from the electrochemical reaction of fuels like hydrogen or carbon monoxide with oxidants like oxygen or air, instead of direct combustion at elevated temperatures. Oxygens are ionized at the cathode/electrolyte interface and transported through vacancies in the electrolyte, a dense ceramic ionic conductor such as stabilized zirconia or ceria, to the anode, where they react with hydrogen to form water; both electrical energy and heat are released during the process. To increase the power density per unit volume, many SOFC developers are pursuing planar designs in which repeating unit cells are stacked and connected electrically in series. A typical planar SOFC stack with internal manifolding is schematically shown in Fig. 1. The repeat unit of the stack is composed of a cell or PEN (positive electrode–electrolyte–negative electrode) sealed onto a metallic frame and separated with metallic interconnects. There are multiple possible sealing locations in a SOFC stack, e.g., S1, S2, S3, and S4 in Fig. 1. S1 represents the seal between the PEN and the metallic frame, S2 is the seal between the metallic interconnect and the metallic cell frame, S3 is the seal between the metallic frame and a ceramic insulating plate (required, for example, if a braze is used in S2), and S4 represents the seal between the end plate and the adjacent cell. It is evident that the sealing in SOFCs can be complex in geometry as well as in the materials to be sealed. As a result a reliable sealant or sealants remains one of the top priorities in advancing planar SOFC technology. Candidate sealant or sealants must show the desired hermeticity or allowable leak rates, and thermal, mechanical, electrical, and

* Corresponding author at: K2-44, PNNL, P.O. Box 999, Richland, WA 99354, United States. Tel.: +1 509 3752527; fax: +1 509 3752186.
E-mail address: yeong-shyung.chou@pnl.gov (Y.-S. Chou).

0378-7753/$ – see front matter © 2007 Published by Elsevier B.V.
doi:10.1016/j.jpowsour.2007.03.039

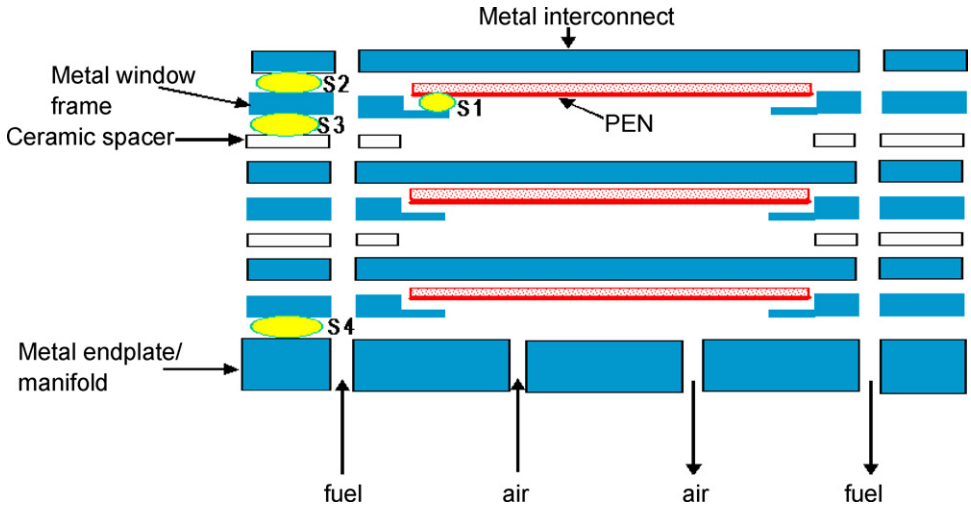

Fig. 1. Schematic showing the multiple sealing sections in planar SOFC stacks. S1 is the seal between the PEN and metallic window frame, S2 is the seal between the metallic interconnect and the window frame, S3 is the seal between an insulator ceramic spacer and the frame, and S4 is the seal between window frame and the endplate.

chemical stability in the harsh SOFC operating conditions, i.e., dual environments of oxidizing and wet reducing gases, for a lifetime up to 40,000 h and numerous thermal cycles [2].

To date, SOFC seal research has been focused mainly on glass/glass-ceramic seals [3–11], as well as compressive mica-based seals [2,12,13] and metallic brazes [14–16]. Due to the thermal cycling involved in routine SOFC operations, the glass and braze approaches require a close match of the coefficients of thermal expansion (CTE) with the mating parts, whereas the compressive mica seals do not. For the current state-of-the-art planar SOFCs, the CTE of the sealing glass should be in the range of $12–13 \times 10^{-6}\,^{\circ}C^{-1}$, which matches closely with the ferritic stainless steels and the Ni-YSZ anode-supported thin electrolyte cells. Currently, alkaline earth based aluminosilicate glasses have been developed and studied as the candidate sealing glasses [4–9,11]. Lahl et al. studied the crystallization kinetics of $AO–Al_2O_3–SiO_2–B_2O_3$ glasses (A = Ba, Ca, Mg) and the influence of nucleating agents [8]. They found that the activation energy of crystal growth was enhanced by most nucleating agents such as TiO_2 and Cr_2O_3 except ZrO_2, and that the preparation method determined whether surface or bulk nucleation was the dominant mechanism. Sohn et al. investigated the thermal and chemical stability of the $BaO–Al_2O_3–La_2O_3–SiO_2–B_2O_3$ system. They found that the CTE increased with BaO content and a maximum CTE of $\sim 11 \times 10^{-6}\,^{\circ}C^{-1}$ was obtained at BaO = 40% and $B_2O_3/SiO_2 = 0.7$ [9]. Ley et al. studied the glass and glass-ceramic system of $SrO–Al_2O_3–La_2O_3–SiO_2–B_2O_3$. The CTE of the as-made materials were in the range of $8–13 \times 10^{-6}\,^{\circ}C^{-1}$, while the long-term stability was not reported [5]. Other systems of phosphate glasses [10], borosilicate glasses [3], and ceramic fiber reinforced glass [4] have also been investigated. However, the CTEs of these glasses were in the low range, e.g., $\sim 5.7–7.9 \times 10^{-6}\,^{\circ}C^{-1}$ for the phosphate glasses [10], and resulted in poor thermal cycle stability. A good example of a state-of-the-art sealing glass is a Ba–Ca–Al–B silicate glass-ceramic developed by Pacific Northwest National Laboratory [17]. This glass has a very good CTE match with the SOFC components after short-term crystallization at 750 °C for 4 h (CTE $\sim 12.5 \times 10^{-6}\,^{\circ}C^{-1}$). The CTE, however, decreases to $\sim 11 \times 10^{-6}\,^{\circ}C^{-1}$ after aging at 750 °C for 1000 h, which could cause problems during repeated thermal cycling. The objective of this study was to investigate a similar Sr–Ca–B silicate glass system with the focus on the effect of a transition metal oxide (NiO) on the thermal and mechanical properties. Nickel oxide was selected due to its high CTE of $\sim 14 \times 10^{-6}\,^{\circ}C^{-1}$ and refractoriness (m.p. $\sim$ 1980 °C). Two approaches were used to incorporate NiO into the glasses. One was a conventional glass making approach (in which the NiO was included in the initial glass melt), while the other was a composite glass approach (in which the NiO was mixed with the glass powders). Both thermal and mechanical properties were measured. Microstructure and the crystalline phases were also examined.

2. Experimental

2.1. Sample preparation by glass and composite approach

The chemical compositions used for the glass approach are listed in Table 1. Four glasses were made with varying NiO content: YSO-1 (NiO = 0 mol%), YSO-11 (NiO = 5%), YSO-12 (NiO = 10%), and YSO-13 (NiO = 15%). Raw materials in the form of powders of SrO (Technical grade), CaO (purity = 95%), B_2O_3 (98.5%), Y_2O_3 and SiO_2 (99.9%), and NiO (99%) (all from Alfa Aesar, Ward Hill, MA) were weighed and dry mixed

Table 1
Chemical compositions of the glass approach in mol%

Glass #/oxides	SrO	NiO	CaO	Y_2O_3	B_2O_3	SiO_2
YSO-1	42.5	0.0	10.0	6.0	7.5	34.0
YSO-11	42.5	5.0	5.0	6.0	7.5	34.0
YSO-12	42.5	10.0	0.0	6.0	7.5	34.0
YSO-13	37.5	15.0	0.0	6.0	7.5	34.0

in a plastic jar for half an hour. The powder mixtures were then placed in a Pt crucible and melted at 1500 °C for half an hour. After melting, the glasses were poured and annealed at 600 °C for 6 h. A small rectangular bar (~25.4 mm long) was cut from the annealed glass for thermal property measurements. The rest of the glass was then crushed and ground in a vibration mill for 2 min. After vibration mill the glass powders were further reduced in size by attrition milling (Szegvari Attritor Model 01HD, Akron OH) in *iso*-propanol for 2 h. After attrition milling, the powder slurry was first dried on a hot plate, followed by drying in an oven at 110 °C for several hours. For the composite approach, NiO powders were directly mixed with glass powders of YSO-1 at volume percents of 5, 10, and 15 for glasses YSO-14, YSO-15, and YSO-16, respectively. The powder mixtures were attrition-milled and dried in the same manner as was used in the glass approach.

After drying, the powders from both approaches were die-pressed into rectangular bars (approximately 45 mm × 16 mm × 5 mm) for sintering. They were slowly fired at 2 °C/min to 550 °C and held for 2 h for organic binder burn-off, followed by heating at 3 °C/min to 1000 °C, where they were held for 1 h. The samples were then cooled at 3 °C/min to 800 °C and held for 4 h before cooling to room temperature. Note that all the heat treatments were conducted in ambient air.

2.2. Thermal properties, mechanical properties and microstructure characterization

Thermal properties including the glass transition temperature (T_g), softening temperature (T_s), and CTE were measured using a dilatometer (Unitherm 1161, ANTER Corp, Pittsburgh, PA) at a heating rate of 2 °C/min in air. For samples from the glass approach, both the annealed glass and sintered powder compacts were measured. For samples from the composite approach only sintered powder compacts were measured. After thermal property measurements, the glass bars were polished on two parallel sides for determination of the elastic properties, i.e., shear (G) and Young's (E) modulus, using the pulse–echo method. The ultrasonic pulse was generated by an ultrasonic source device (Sonic 137, Staveley, Kennewick, WA) and the echo signals were recorded by an oscilloscope (Tektronix TDS220, Beaverton, OR). Specimens were also mounted in epoxy and polished for microstructure characterization with scanning electron microscopy (SEM). The remaining sections of the sintered bars were then crushed with a pestle and mortar and sieved through a Tyler scale 325 mesh for phase characterization by X-ray diffraction (Phillips XRG3000).

3. Results and discussion

3.1. Effect of NiO on the glass making

As mentioned earlier, a rigid hermetic seal such as a glass-ceramic seal requires close CTE match with the mating SOFC components, typically in the range of 12–13 × 10^{-6} °C^{-1}. Common alkaline-earth silicate glasses have low CTEs except for high Ba-content silicate glasses [9,17]. In this work, NiO was proposed as an additive to increase the CTE of a novel Sr-silicate glass due to its relatively high CTE (~14 × 10^{-6} °C^{-1}) among common oxides, assuming that NiO would remain as a separate phase in the glass instead of forming compounds with other oxide constituents of the glass. In addition, it has good chemical compatibility with the YSZ electrolyte since it is widely used as the anode material. Four glasses were prepared with varying NiO content and their compositions are listed in Table 1. Higher NiO content glasses were not considered due to the potential to reach the percolation limit, which could result in high electrical conductivity if the free NiO was reduced to Ni metal during long-term exposure in the reducing environment For these glasses, the total contents of SrO + NiO + CaO were kept constant at 52.5 mol%. The balance of the compositions was also fixed. It was found that the parent glass (YSO-1, NiO = 0%) was completely transparent and colorless after casting and annealing. No bulk or surface precipitates or crystallization products were found, indicating good glass forming and homogeneous in chemical compositions. Upon the addition of NiO, the glasses became glossy black. Streaks of green precipitation appeared on the surface and became more apparent as the amount of NiO increased. After cutting of the annealed glasses prepare CTE bars, a heterogeneous mixture of black and green streaks was also evident through the thickness of the glass, especially in glass YSO-13 where the NiO content was the highest (15%). This suggests that the solubility limit of NiO in the parent glass had been reached although no published data or phase diagrams were available for this complex alkaline-earth silicate glass system. It was also noted that higher NiO content glasses (YSO-13, NiO = 15%) appeared to be more brittle and readily fractured into multiple pieces upon cutting for CTE bars, possibly because of residual stresses during cooling caused by the presence of the bulk precipitates/crystallization products. To determine the precipitates/crystallization products, X-ray powder diffraction analysis was performed on the higher NiO glasses (YSO-12 and YSO-13). For comparison, the parent glass YSO-1 was also analyzed. The powder diffraction patterns of the as-cast and annealed glasses are shown in Fig. 2. Clearly, all glasses showed similar patterns of an amorphous nature with very low intensity,

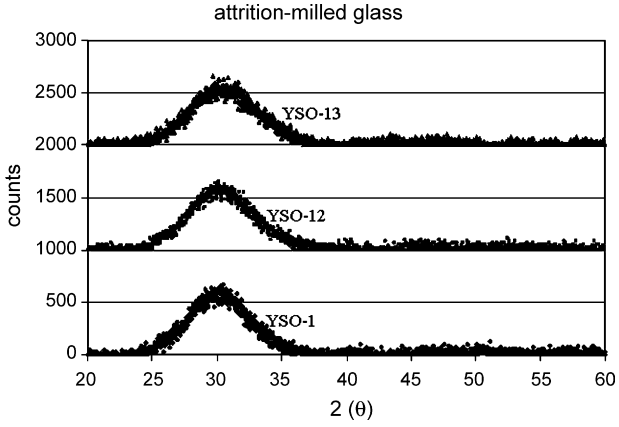

Fig. 2. XRD powder diffraction patterns of glasses YSO-1 (NiO = 0%), YSO-12 (NiO = 10 mol%), and YSO-13 (NiO = 15 mol%) showing the amorphous nature of the glass.

Table 2
Thermal and mechanical properties of the annealed glass

Glass #	NiO (mol%)	Density (g cm^{-3})	E (GPa)	G (GPa)	ν	T_g (°C)	T_s (°C)	CTE ($\times 10^{-6}$ °C^{-1})
YSO-1	0	3.80	96.6	37.3	.30	698	735	12.09
YSO-11	5	3.92	84.4	32.1	.31	675	725	11.79
YSO-12	10	3.99	90.4	34.6	.31	683	730	11.45
YSO-13	15	4.06	96.1	36.5	.32	683	730	11.48

Note: CTE was averaged from room temperature to T_g.

including the glasses with high NiO contents and an appreciable amount of precipitates. This may suggest the precipitates were either amorphous in nature or very fine in particle size.

3.2. Effect of NiO on the mechanical and thermal properties of sintered glass by glass approach

The mechanical and thermal properties of the annealed glasses from the glass approach are summarized in Table 2; densities are also included. It was found that the higher the NiO content, the greater the density of the glasses. The density increased from 3.82 g cm^{-3} for glass YSO-1 (NiO = 0%), to 3.92 g cm^{-3} for glass YSO-11 (NiO = 5%), 3.99 g cm^{-3} for glass YSO-12 (NiO = 10%), and to 4.06 g cm^{-3} for glass YSO-13 (NiO = 15%). This is not surprising since NiO has a higher density (~6.72 g cm^{-3}) than most silicate glasses. For the elastic modulus, the trend with increasing NiO content was different. At low NiO (5%) content (glass YSO-11), the shear modulus = 32.1 GPa and Young's modulus = 84.4 GPa. These were both lower than the values of the parent glass YSO-1, i.e., shear modulus = 37.3 GPa and Young's modulus = 96.6 GPa. However, with increasing NiO content the elastic moduli increased. Glass YSO-12 (NiO = 10%) had a shear modulus of 34.6 GPa and Young's modulus of 90.4 GPa, and the shear and Young's moduli of glass YSO-13 (NiO = 15%) were 36.5 GPa and 96.1 GPa, respectively. The cause for lower elastic moduli at NiO = 5% was not clear since NiO has a higher elastic modulus than common silicate glasses. For example, the shear and Young's moduli of fully dense NiO were determined to be 84 and 220 GPa, respectively [18]. Young's modulus of most common commercial silicate glasses varies from about 50 GPa for low-T_g glass to about 75 GPa for fused SiO_2 and E-glass fiber. Some special glasses (S-glass of magnesium aluminosilicate composition) have a higher modulus about 85–90 GPa. Some ternary silicate glasses ($CaO–Al_2O_3–SiO_2$) even have a Young's modulus close to 100 GPa and shear modulus of 35–38 GPa [19]. The glasses in the present study were in the same range as these ternary glasses.

Appropriate linear thermal expansion coefficients are primary targets in developing sealing glasses. A matching CTE is important both in the glassy state during sealing and initial stage of SOFC operations, and in the crystallized state during mid- and long-term operations as the amorphous glass transitions into a glass-ceramic. This is true especially for transportation applications where SOFC stack is to be used as an auxiliary power unit and must survive frequent thermal cycles shortly after sealing during routine day-to-day operation. Some stationary applications may be more forgiving in that the average CTE in the glassy state during sealing and the partially crystallized state during the initial stage of operation (e.g., a few hundred or thousand hours) may not be required to closely match with SOFC stack components, because thermal cycling may not occur in the initial stages of operation. Even in this case, however, the system will likely need to be stopped for periodic maintenance so that some thermal cycles would be required in the mid to long-term stage of operations. Linear expansion curves of the glasses with the lowest and highest NiO contents (glass YSO-1 and YSO-13) are shown in Fig. 3 for the as-cast and annealed glass, and in Fig. 4 for the sintered glasses. Glasses YSO-11 and YSO-12 with intermediate NiO contents behaved similarly and are not

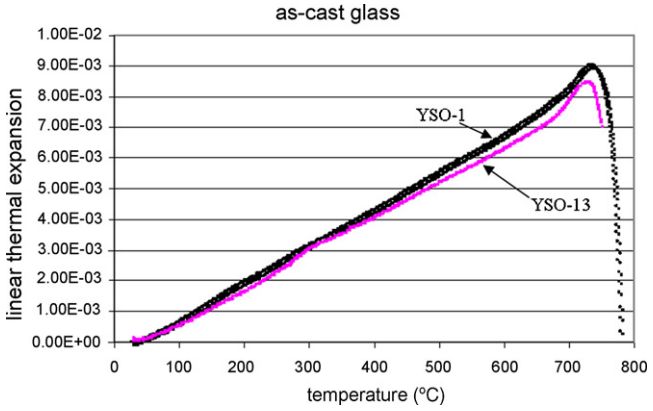

Fig. 3. Linear thermal expansion curves of as-prepared glasses YSO-1 (NiO = 0%) and YSO-13 (NiO = 15%).

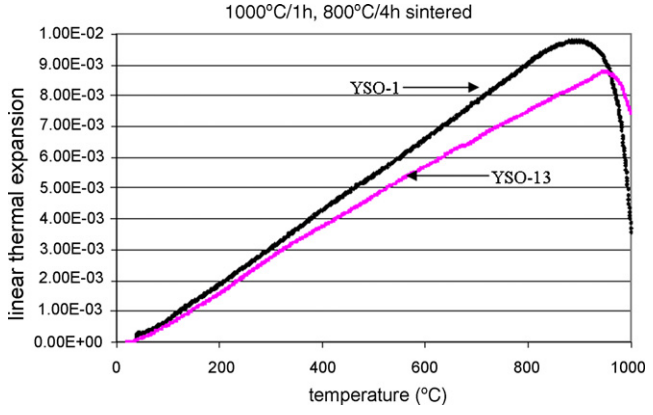

Fig. 4. Linear thermal expansion curves of glasses YSO-1 (NiO = 0%) and YSO-13 (NiO = 15%) sintered at 1000 °C/1 h and 800 °C/4 h in air using attrition-milled powders.

shown in these figures. In Fig. 3, the linear expansion curves are very similar for both glasses and the thermal expansion is approximately linear up to the glass transition point where the expansion rapidly increased till the softening point. The glass transition point, softening point, and the average (from room temperature to T_g) CTE are listed in Table 2. It was found that the addition of NiO appeared to slightly decrease the glass transition and softening points. For example, T_g decreased from 698 °C (YSO-1) to 675 for YSO-11, and 683 °C for both YSO-12 and YSO-13. T_s decreased from 735 °C (YSO-1) to 725 °C for YSO-11 and 730 °C for both YSO-12 and YSO-13. For the CTE, a similar trend was observed in that the addition of NiO resulted in slightly lower values. For example, the average CTE of the parent glass YSO-1 was $\sim 12.1 \times 10^{-6}\,°C^{-1}$. It was $\sim 11.8 \times 10^{-6}\,°C^{-1}$ for glass YSO-11, $\sim 11.5 \times 10^{-6}\,°C^{-1}$ for glass YSO-12 and $\sim 11.5 \times 10^{-6}\,°C^{-1}$ for glass YSO-13. Overall, among the thermal properties, glasses YSO-12 and YSO-13 seemed to have very similar values. This appeared to be consistent with the observations that these glasses showed some precipitation/crystallization upon glass making, indicating that a solubility limit had been reached (the precipitates were unable to identify by XRD as mentioned in previous section). As a result, further change in glass formulations likely did not change substantially the chemical compositions of the vitreous glass matrix, and hence the thermal properties remained the same. This would not be the case for the mechanical properties and density since all the constituents of the glass (vitreous glass matrix or matrices and precipitates) would contribute.

For the sintered samples in which glass powder compacts were fired to 1000 °C/1 h followed by 800 °C/4 h, the linear thermal expansion curves are shown in Fig. 4 for the parent glass (YSO-1) and the highest NiO content glass (YSO-13). Again, glasses (YSO-11 and YSO-12) with intermediate NiO contents showed similar behavior and were not included in the figure. The sintered powder compacts showed extensive fracturing that prevented the measurement of their mechanical properties. Both macro (in mm) and micro-cracks (in μm) were present as shown in Fig. 5A and B, respectively. It will be noted that the micro-cracks appear to be radial (as contrast to circumferential) from the elongated grains (arrows in Fig. 5B) suggesting this phase had lower CTE than the surrounding matrix. EDS analysis of these elongated grains indicated high Y content along with small amounts of Sr and Si. This phase was later confirmed by XRD to be YBO_3 (B was undetectable by the EDS system). The small white particles in Fig. 5B were NiO. The cracking appeared to be more severe for higher NiO contents, presumably due to more of the YBO_3 phase being present. Microstructure and phase analysis will be discussed later this paper. Bulk density, T_s, and average CTEs of the sintered glasses are listed in Table 3. Glass YSO-12 and YSO-13 appeared to have lower bulk density than YSO-11 and was expected due to more cracks. Softening points of the sintered glasses were $T_s = 903$ °C for YSO-1, $T_s = 900$ °C for YSO-11, $T_s = 950$ °C for YSO-12, and $T_s = 955$ °C for YSO-13. The presence of dilatometric softening points for the sintered glasses clearly indicated the presence of residual glass after the sintering processes. However, the amount of residual glass was much smaller, as evidenced by

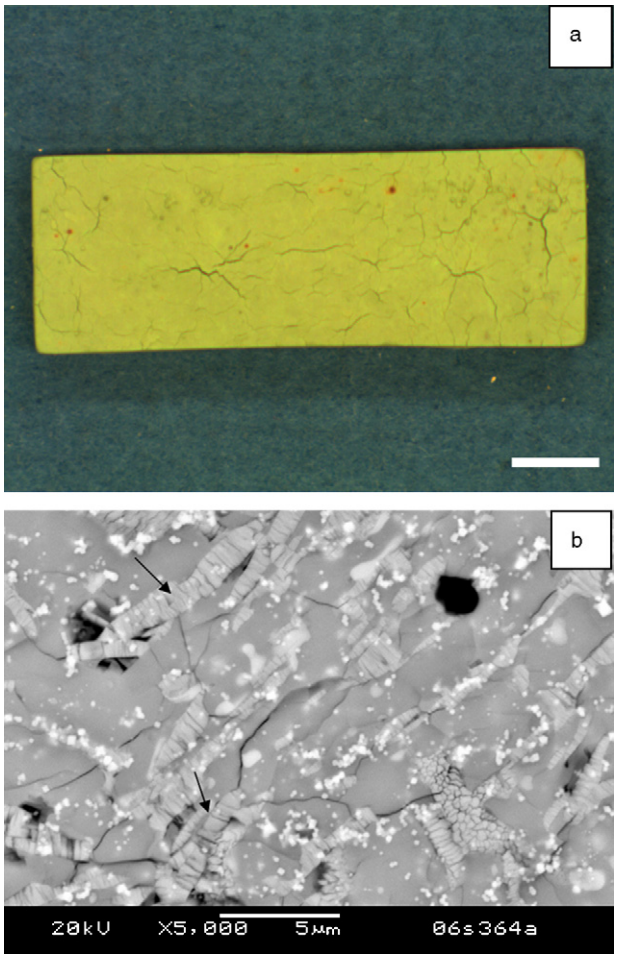

Fig. 5. Morphology of the sintered glass showing (A) macro cracks (bar = 5 mm) and (B) micro-cracks of glass YSO-12. Arrows in (B) showed the elongated grains where radial micro-cracks formed. The small white particles were NiO.

the fact that the softening occurred over a broader temperature range and the lack of distinct of T_g in Fig. 4 as compared to the more sharp and narrow range in the annealed glasses (Fig. 3). The average (from room temperature to T_s) CTEs were $\sim 11.7 \times 10^{-6}\,°C^{-1}$ (YSO-1), $\sim 11.9 \times 10^{-6}\,°C^{-1}$ (YSO-11), $\sim 9.8 \times 10^{-6}\,°C^{-1}$ (YSO-12), and $\sim 9.8 \times 10^{-6}\,°C^{-1}$ (YSO-13). The significant decrease (~17%) in CTE for the highest NiO content glass (YSO-13) from the parent glass (YSO-1) was surprising since the addition of NiO was expected to increase CTE, as observed in YSO-11 with 5% NiO. The lower CTEs for glasses YSO-12 and YSO-13 were likely due to the formation of YBO_3 phases. No published CTE data of YBO_3 was available;

Table 3
Thermal and mechanical properties of the sintered glass by the glass approach

Glass #	NiO (mol%)	Bulk density ($g\,cm^{-3}$)	T_s (°C)	CTE ($\times 10^{-6}\,°C^{-1}$)
YSO-1	0	3.43	903	11.73
YSO-11	5	3.50	900	11.91
YSO-12	10	3.26	950	9.85
YSO-13	15	3.20	955	9.77

Note: CTE was averaged from room temperature to T_s.

however, CTE of a ternary YAB (Y_2O_3–Al_2O_3–B_2O_3) glass was in the range of 6.4–7.5 × 10^{-6} °C^{-1} (average of 200–600 °C) [20].

3.3. Effect of NiO on the thermal and mechanical properties of sintered glass of the composite approach

In this study, we also investigated a composite glass approach in developing sealing glasses with high CTEs. The composite glass approach as compared to the glass making approach had the potential advantage of allowing a wider range of NiO addition into the glass (and maintenance of NiO as a separate phase in the glass) since the composite glass would not experience the high temperature (i.e., 1500 °C) required to make the glass from a molten oxide mixture, which would tend to promote reaction of NiO with other constituents. Instead, the typical process (sealing) temperatures for the composite glass approach were lower (<1050 °C), much less than the melting point of NiO (~1980 °C) or the stable compound in the NiO–SiO_2 system (Ni_2SiO_4 ~1545 °C) [21]. However, there were potential issues such as micro residual stresses around NiO particles, which have higher CTE than the glass matrix or the crystallized phases. These residual stresses could result in circumferential micro-cracking around NiO particles if a critical NiO size was reached and high stresses were not be relieved by the surrounding glass matrix. However, unlike the sintered glasses prepared via the glass approach, the three composite glasses, including the highest NiO addition at 15 vol.% (27.1 mol%), showed no macro and micro-cracking after the same heat treatment.

The mechanical and thermal properties of the sintered composites are listed in Table 4, as well as the sintered densities. There was no apparent trend in the mechanical properties in terms of the NiO content, though all the three composite glasses had higher moduli than the parent glass. For example, the Young's modulus of the sintered parent glass (YSO-1) was 98.1 GPa, compared to 117.2 GPa for composite YSO-14 (NiO = 5 vol.% or 9.9 mol%), 120.9 GPa for composite YSO-15 (NiO = 10 vol.% or 18.9 mol%), and 103.9 GPa for composite YSO-16 (NiO = 15 vol.% or 27.1 mol%). No comparison was possible with the sintered glasses prepared by the glass approach since those glasses were fractured after sintering and therefore no elastic property measurements were conducted. As for the thermal properties, higher NiO content appeared to result in higher CTEs. The average CTE of glass YSO-14 (NiO = 5 vol.%) was 11.74 × 10^{-6} °C^{-1}, glass YSO-15 (10 vol.%) was 12.01 × 10^{-6} °C^{-1}, and glass YSO-16 (15 vol.%) was 12.16 × 10^{-6} °C^{-1}. T_s increased from ~920 °C for NiO = 5 vol.% to ~925 °C for 10 vol.%, and to 945 °C for 15 vol.%, consistent with more NiO (higher m.p.) or less glass in the composites.

It was proposed by Turner that the CTE of a ceramic composite can be expressed by rule of mixture with the following equation [22]:

$$\alpha_{\text{composite}} = \frac{\alpha_1 K_1 W_1/\rho_1 + \alpha_2 K_2 W_2/\rho_2}{K_1 W_1/\rho_1 + K_2 W_2/\rho_2} \quad (1)$$

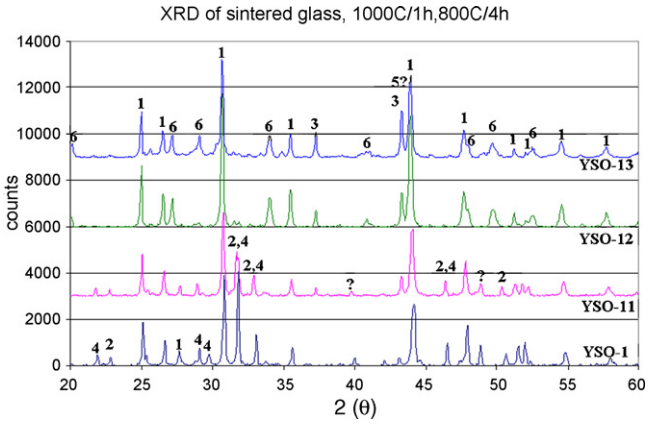

Fig. 6. XRD patterns of the glasses YSO-1 (NiO = 0 mol%), YSO-11 (NiO = 5 mol%), YSO-12 (NiO = 10 mol%), and YSO-13 (NiO = 15 mol%) sintered at 1000 °C/1 h followed by 800 °C/4 h in air. The numbers in the patterns represent the following crystalline phases: (1) $SrSiO_3$, (2) Ca_2SiO_4, (3) NiO, (4) Ca_3SiO_5, (5) $SrNiO_3$ and (6) YBO_3.

where α is the CTE, K represents the bulk modulus, W the weight fraction, and ρ is the density. Subscripts 1 and 2 represent phase 1 and phase 2 in the mixture. The major assumption in Eq. (1) was that no new phase formed between individual phases. Given the known physical properties of parent glass YSO-1 and NiO, the theoretical CTEs of the composite were calculated to be 12.1 × 10^{-6} °C^{-1} (NiO = 5 vol.%), 12.3 × 10^{-6} °C^{-1} (10 vol.%), and 12.6 × 10^{-6} °C^{-1} (15 vol.%) (Table 4). The measured values showed good agreement with the theoretical ones. The difference was ranged from 2.7 to 3.3%, suggesting minimal reactions between NiO and the parent glass. The details of phase characterization will be discussed in the next section.

3.4. Microstructure and phase characterization

Microstructure and phase characterization were performed in order to understand the discrepancy apparent in the decrease of CTE with increasing NiO content in the melting glass approach and the increase in CTE for the composite approach. Fig. 6 shows the diffraction patterns of the sintered glasses from the glass approach (YSO-1 and YSO-11 to YSO-13). All the glasses were subjected to the same thermal processes. The major phase in these glasses was monoclinic $SrSiO_3$. The minor phases appeared to vary. For glass YSO-1 and YSO-11, calcium silicates of Ca_2SiO_4 and Ca_3SiO_5 were identified. Calcium silicate formation was not possible for glasses YSO-12 and YSO-13 since CaO was not used in those glasses. As more NiO was added, the peak intensity of NiO was more evident (peak #3 in Fig. 6) and another minor phase, YBO_3, was present (peak #6). In these patterns no Ni_2SiO_4 (nickel olivine) was found, which is the only stable compound in the NiO–SiO_2 binary system as shown in Fig. 7 [21]. Nickel olivine is not stable at temperature above 1545 °C since it will decompose into NiO and cristobalite. The silicate glass system is this study was more complicated than that simple binary system; no ternary or quaternary systems were available. Thermodynamic calculations using the HSC Chemistry 5 software was therefore conducted to study the

Table 4
Thermal and mechanical properties of the sintered glass by the composite approach

Glass #	NiO (vol%)	NiO (mol%)	Bulk density ($g\,cm^{-3}$)	E (GPa)	G (GPa)	ν	T_s (°C)	Theoretical CTE ($\times10^{-6}\,°C^{-1}$)	Measured CTE ($\times10^{-6}\,°C^{-1}$)
YSO-1	0	0	3.43	98.1	37.7	.30	903	–	11.73
YSO-14	5	9.9	3.89	117.2	45.8	.28	920	12.06	11.74
YSO-15	10	18.9	4.00	120.9	47.4	.27	925	12.34	12.01
YSO-16	15	27.1	3.98	103.9	40.4	.28	945	12.57	12.16

Note: CTE was averaged from room temperature to T_s.

formation of the observed crystalline phases. Based on available thermodynamic properties, the Gibbs free energy of the following reactions was calculated for two temperatures (800 and 1500 °C):

$$SrO + SiO_2 \rightarrow SrSiO_3, \quad \Delta G = -132\,kJ\,mol^{-1}\,(800\,°C), \; -133\,kJ\,mol^{-1}\,(1500\,°C) \tag{2}$$

$$2CaO + SiO_2 \rightarrow Ca_2SiO_4, \quad \Delta G = -137\,kJ\,mol^{-1}\,(800\,°C), \; -150\,kJ\,mol^{-1}\,(1500\,°C) \tag{3}$$

$$3CaO + SiO_2 \rightarrow Ca_3SiO_5, \quad \Delta G = -170\,kJ\,mol^{-1}\,(800\,°C), \; -186\,kJ\,mol^{-1}\,(1500\,°C) \tag{4}$$

$$2NiO + SiO_2 \rightarrow Ni_2SiO_4, \quad \Delta G = -5.5\,kJ\,mol^{-1}\,(800\,°C), \; -2.9\,kJ\,mol^{-1}\,(1500\,°C) \tag{5}$$

It is apparent that $SrSiO_3$, Ca_2SiO_4 and Ca_3SiO_5 are thermodynamically more favorable than Ni_2SiO_4 to form between these two temperatures, which is consistent with the observed crystalline phases in the sintered glasses. Calculations for YBO_3 were not conducted due to lack of thermodynamic data, and it was unclear why YBO_3 did not form in glasses YSO-1 and YSO-11. The trend of increasing NiO peaks with increasing NiO content in the glasses was also evident, suggesting no significant reaction between NiO and SiO_2 or other species in the glasses. The XRD results clearly demonstrated the desired chemical compatibility of NiO in the current glass system.

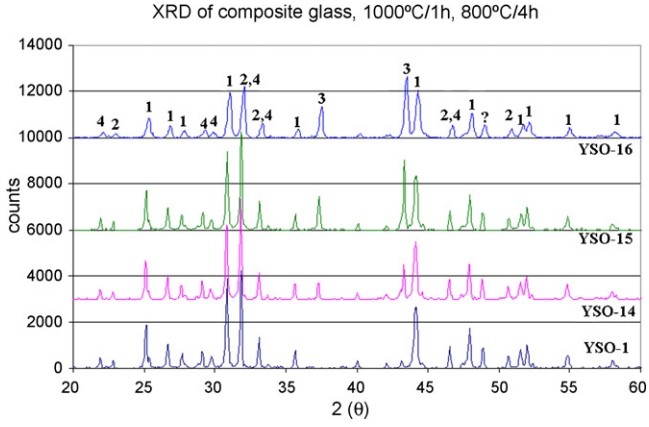

Fig. 7. XRD patterns of the composite glasses YSO-1, YSO-14, YSO-15, and YSO-16 sintered at 1000 °C/1 h followed by 800 °C/4 h in air. The numbers in the patterns represent the following crystalline phases: (1) $SrSiO_3$, (2) Ca_2SiO_4, (3) NiO and (4) Ca_3SiO_5.

For the composite glass approach (Fig. 7), it is apparent that the addition of NiO did not alter the crystalline phases of the parent glass (YSO-1). The major phase was $SrSiO_3$ with minor amounts of Ca_2SiO_4, Ca_3SiO_5, and NiO. No Ni_2SiO_4 was detected and NiO peaks showed increase intensity with increasing NiO addition, consistent with the CTE measurements.

4. Summary and conclusions

A novel Sr-silicate sealing glass for SOFC was developed with a focus on the effects of NiO on glass forming, thermal, and mechanical properties. Two approaches were tested: inclusion of NiO in the glass melt and a glass/NiO composite. In the glass making approach, no distinct trend was found for the thermal and mechanical properties with increasing NiO content. CTE of sintered compacts of glass powder with high (10–15 mol%) NiO contents showed a substantial drop from the parent glass, and extensive macro- and micro-cracking were observed. Possible causes were discussed and were attributed to the formation of YBO_3. In the composite glass approach, CTEs of the sintered powder compacts increased with increasing NiO content from $11.7 \times 10^{-6}\,°C^{-1}$ (5 vol.% NiO) to $12.0 \times 10^{-6}\,°C^{-1}$ (10 vol.%), and to $12.2 \times 10^{-6}\,°C^{-1}$ (15 vol.%). Rule of mixture predictions were consistent with the measured values. The phases present were characterized with XRD; the presence of NiO phase instead of reaction products indicated the desired chemical compatibility of NiO with the glass. Coupon sealing and interfacial microstructure and chemical analysis will be addressed in the second paper. Overall, the composite glass approach with NiO demonstrated a viable way to tailor thermal and mechanical properties of candidate SOFC sealing glasses.

Acknowledgements

The authors would like to thank S. Carlson and J. Coleman for SEM sample preparation and analysis. This paper was funded as part of the Solid-State Energy Conversion Alliance (SECA) Core Technology Program by the US Department of Energy's National Energy Technology Laboratory (NETL). Pacific Northwest National Laboratory is operated by Battelle Memorial Institute for the US Department of Energy under Contract no. DE-AC06-76RLO 1830. Robert Gow would also like to acknowledge the U.S. DOE, Office of Science's Community College Initiative, CCI Program, his mentor, Dr. Yeong-Shyung

Chou, and other PNNL employees for their help during his summer internship.

References

[1] N.Q. Minh, J. Am. Ceram. Soc. 76 (3) (1993) 563–588.
[2] Y.S. Chou, J.W. Stevenson, J. Mater. Eng. Perform. 15 (4) (2006) 414–421.
[3] X. Qi, F.T. Akin, Y.S. Lin, J. Membr. Sci. 193 (2001) 185–193.
[4] S. Taniguchi, M. Kadowaki, T. Yasuo, Y. Akiyama, Y. Miyake, K. Nishio, J. Power Sources 90 (2000) 163–169.
[5] K.L. Ley, M. Krumpelt, R. Kumar, J.h. Meiser, I. Bloom, J. Mater. Res. 11 (6) (1996) 1489–1493.
[6] V.A.C. Haanappel, V. Shemet, I.C. Vinke, S.M. Gross, T.H. Koppitz, N.H. Menzler, M. Zahid, W.J. Quadakkers, J. Mater. Sci. 40 (2005) 1583–1592.
[7] N. Lahl, D. Bahadur, K. Singh, L. Singheiser, K. Hilpert, J. Electrochem. Soc. 149 (5) (2002) A607–A614.
[8] N. Lahl, K. Singh, L. Singheiser, K. Hilpert, D. Bahadur, J. Mater. Sci. 35 (2000) 3089–3096.
[9] S.-B. Sohn, S.-Y. Choi, G.-H. Kim, H.-S. Song, G.-D. Kim, J. Non-Crystalline Solids 297 (2002) 103–112.
[10] P.H. Larsen, P.F. James, J. Mater. Sci. 33 (1998) 2499–2507.
[11] Z. Yang, J.W. Stevenson, K.D. Meinhardt, Solid State Ionics 160 (2003) 213–225.
[12] Y.S. Chou, J.W. Stevenson, J. Power Sources 112 (2002) 376–383.
[13] Y.S. Chou, J.W. Stevenson, J. Power Sources 140 (2005) 340–345.
[14] K.S. Weil, J.S. Hardy, J.Y. Kim, J. Adv. Special. Mater. V Am. Soc. Met. 5 (2000) 47–55.
[15] J. Duquette, A. Petric, J. Power Sources 137 (2004) 71–75.
[16] K.S. Weil, J.Y. Kim, J.S. Hardy, Electrochem. Solid State Lett. 8 (2005) A133–A136.
[17] K.D. Meinhardt, L.R. Pederson, US Patent 6,430,966 (2002).
[18] C. Liu, A. Huntz, J. Lebrun, Mater. Sci. Eng. A 160 (1993) 113.
[19] O.V. Mazurin, M.V. Streltsina, T.P. Shvaiko-Shvaokovskaya (Eds.), Handbook of Glass Data, Part C Ternary Silicate Glasses, Physical Science Data, vol. 15, Publisher Elsevier, 1987, p. 802.
[20] H.L. Rutz, D.E. Day, C.F. Spencer Jr., J. Am. Ceram. Soc. 73 (6) (1990) 1788–1790.
[21] B. Phillips, J.J. Hutta, I. Warshaw, J. Am. Ceram. Soc. 46 (12) (1963) 579–583.
[22] P.S. Turner, J. Res. NBS 37 (1946) 239.